Journal of Petroleum Science and Engineering 161 (2018) 291–301

Contents lists available at ScienceDirect

Journal of Petroleum Science and Engineering

journal homepage: www.elsevier.com/locate/petrol

Evaluating shale oil in the Dongying Depression, Bohai Bay Basin, China, using the oversaturation zone method

Yan-Rong Zou [a,*], Jia-Nan Sun [a,b], Zheng Li [c,d], Xingyou Xu [d], Maowen Li [e], Ping'an Peng [a]

[a] State Key Laboratory of Organic Geochemistry, Guangzhou Institute of Geochemistry, Chinese Academy of Sciences, Guangzhou, 510640, China
[b] University of Chinese Academy of Sciences, Beijing 10039, China
[c] State Key Laboratory of Oil and Gas Reservoir Geology and Exploitation, Chengdu University of Technology, Chengdu, Sichuan 610059, China
[d] Geology Scientific Research Institute of Shengli Oilfield Company, SINOPEC, Dongying, 257015, China
[e] Sinopec Key Laboratory of Petroleum Accumulation Mechanisms, Wuxi Research Institute of Petroleum Geology, Wuxi, 214126, China

ARTICLE INFO

Keywords:
Shale oil
Assessment
Dongying depression
Bohai Bay Basin

ABSTRACT

Increasing energy demands resulting in the need for unconventional shale oil-gas resources are attracting ever more attention. However, although some studies have been conducted on unconventional shale oil resources, little work to date has been carried out on the potential of lacustrine mudstones and shale. In the Dongying Depression of the Bohai Bay Basin, China, significant amounts of oil have been recorded from more than one hundred wells, and flow has been verified in more than ten during conventional petroleum exploration. Because three boreholes aimed at exploring for shale oil have recently been drilled in this depression, we describe here the characteristics of lacustrine mudstones and shale and provide a preliminary assessment of the three wells using the oil sorption index and the oversaturation zone. The results of this study show that the three wells exhibit good potential for shale oil and further suggestions for exploration are presented. We also discuss a number of unusual phenomena discovered in these shale borehole profiles as well as future predictions for the potential distribution of shale oil.

1. Introduction

The Dongying Depression (DD) is located in the southeastern region of the Bohai Bay Basin (BBB), eastern China, and is divided into four sags encompassing 5700 km^2 along a northeast-southwest extended axis (Fig. 1). Although 32 oil and two gas fields have so far been discovered within the DD, there is considerable additional potential for recoverable resources from Paleogene shales (Zhang et al., 2012a).

In 1963, Well Xin3 was blown out by shale oil and gas when a borehole was drilled into the Es3x shale member of the Shahejie Formation during conventional oil exploration. This event marked the first time that petroleum was observed in mudstones and shale source rocks within the DD. Ten years later, fractured shale oil production started from Well He54 in the Es3x member, reaching 91.4 metric tons per day and a cumulative production of 27,896 tons (Zhang et al., 2014). Towards the end of 2011, significant shale oil potential was discovered in Es3 and Es4 shales in 110 wells across the depression (Zhang et al., 2012b, 2014), and to date flow has been achieved from 12 wells in the DD (Wang et al., 2013), two-thirds of which are drilled into the Es4 shale member of the Shahejie Formation (Table 1).

Most recently, three boreholes specifically for shale oil (i.e., NY1, LY1, and FY1) were drilled into three sags (Fig. 1) within the DD. We present preliminary assessment of these wells in this paper.

2. Geological setting

The DD is a half-graben structure located in the middle of the Jiyang sub-basin of the BBB, a Meso-Cenozoic rift basin that developed on a paleotopographical background of Paleozoic basement rocks. A two-stage evolutionary model for the DD is commonly accepted, comprising Paleogene syn-rifting and differential subsidence, followed by a Neogene post-rift phase associated with thermal subsidence (Allen et al., 1997).

The Paleogene syn-rift stage of formation comprised four rifting episodes (Feng et al., 2013), early-initial rifting that began in the Paleocene and ended in the early Eocene, late-initial rifting in the middle Eocene, a rift climax in the late Eocene, and weakened rifting during the Oligocene. Paleogene strata (Fig. 2) in the DD consist of the Kongdian Formation (Ek) which is overlain by the Shahejie Formation (Es), itself overlain by

* Corresponding author.
E-mail address: zouyr@gig.ac.cn (Y.-R. Zou).

https://doi.org/10.1016/j.petrol.2017.11.059
Received 30 October 2016; Received in revised form 28 October 2017; Accepted 22 November 2017
Available online 24 November 2017
0920-4105/

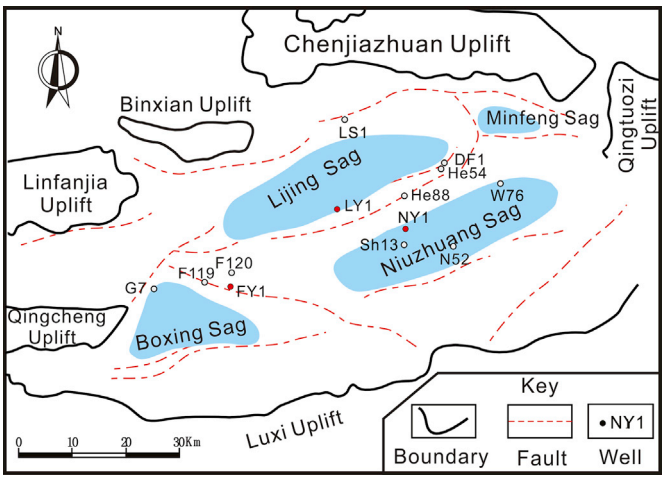

Fig. 1. Geological frame map showing the uplifts, sags, main faults, shale oil well locations, the discovered shale oil flow wells during conventional oil exploration included.

the Dongying Formation (Ed). These Paleogene syn-rift strata form the major hydrocarbon source rocks within the DD; the third basal member of the Shahejie Formation (Es3) is further divided into three sub-members (Fig. 2), with the lowest portion of the third member (Es3x) and the upper portion of the fourth member (Es4s) is generally considered being the main source rocks (Fig. 2). Indeed, commercially viable shale oil flows have mainly been discovered in the Es3x and Es4s members (Zhang et al., 2012a,b; Wang et al., 2013).

The lower portion of the fourth member of the Shahejie Formation (Es4x) consists of alternating layers of red sandstones and mudstones interbedded with saline deposits, implying a shallow salt water lake sedimentary environment (Feng et al., 2013). In contrast, the upper strata that comprise this formation (Es4s) are composed of gray mudstones, oil shales intercalated with sandstones, and thin limestone layers that were deposited in a semi-enclosed saline lake setting (Zhang et al., 2012a; Wang et al., 2013). The lithology of the Es3x member is comprised of dark gray mudstones, oil shales, and dark gray limey mudstones, which imply a deep freshwater lake sedimentary environment (Zhang et al., 2012a; Feng et al., 2013; Wang et al., 2013). The Es3x and the Es4s members are further divided into four and three subordinate sub-members, respectively. Three shale oil boreholes have been drilled into the different strata of these sub-members in order to identify horizons for potential future development.

3. Materials and methods

A total of 434 core samples were collected at about 2 m intervals from the three shale oil boreholes in the DD (Table 2). The core samples were at once freezed in a refrigerator when they were taken out from the borehole in order to reduce the loss of Rock-Eval S_1. The core samples were ground in liquid nitrogen. These samples were analyzed using a Leco C230 carbon analyzer, and TOC frequency distributions are shown in Fig. 3. Rock-Eval pyrolysis was then performed on the core samples ground in liquid nitrogen using Rock Eval 6 following procedure described by Espitalie et al. (1985) with the pyrolysis data generated are S1, S2, Tmax.

The process of adsorption plays a very significant role in unconventional resource plays (Jarvie, 2012b), and a number of experiments on organic matter and the minerals in shale have been reported previously (Wei et al., 2012; Li et al., 2016). In this paper, oil, adsorption experiments on kerogen and minerals separated from shales were carried out to determine oil sorption potential following experimental procedure by Li et al. (2016), allowing subsurface shale sorption to be reconstructed according to shale percentage and the variation in specific surface (i.e., porosity) of subsurface shale. Shale adsorption potential can this be expressed as follows:

$$S_p = p_o x_o + \left[\frac{\varphi}{\varphi_0}\right]^{2/3} \sum_{i=1}^{n} p_i x_i \quad (1)$$

In this expression, $s_p$denotes the shale adsorption potential,p_0 and x_0 refer to the fraction and adsorption capacity of organic matter, respectively, p_i and p_x refer to the i-th mineral fraction and its adsorption capacity in shale, respectively, and are present and initial porosity, respectively, φ and φ_0 the constraint variable $p_0 + \sum_{i=1}^{n} p_i = 1$.

4. Geochemical characteristics

4.1. Bulk organic geochemistry

Total organic carbon (TOC, expressed as weight percent, %), including both kerogen and bitumen, describes the quantity of organic carbon in a rock sample (Peters and Cassa, 1994). Thus, TOC content can be considered to be a direct measure of the amount of carbon present in a petroleum source rock even though it does not provide a clear indication of petroleum potential. The organic richness (TOC) of samples was subdivided into categories <0.5, 0.5–1.0, 1.0–2.0, 2.0–4.0, and >4.0 corresponding to 'poor', 'fair', 'good', 'very good', and 'excellent' levels of TOC (Peters and Cassa, 1994). Thus, results show that percentages of 'good', 'very good', and 'excellent' TOC samples in Es3x member source rocks are 12%, 70%, and 18%, respectively, while percentages of 'good', 'very good', and 'excellent' samples in Es4s member source rocks are 33%, 56%, and 9%, respectively. These data indicate that these samples can be characterized as 'good' to 'excellent' source rocks, with less than 2% classified as just 'fair' in terms of TOC content.

The values of genetic potential (GP) are usually used to evaluate the quality of prospective organic matter in a source rock. On the basis of the

Table 1
Shale oil flow wells of Dongying Depression.

No.	Sag	Well	Strata symbol	Depth (m)	Shale oil production (t/d)	Gas production (m^3/d)
1	Boxing	F119	Es4s	3238.7–3253.1	15.90	0.15
2	Boxing	F119	Es4s	3290.7–3302.1	9.61	0.52
3	Boxing	F120	Es3x	3088–3111	5.14	0
4	Boxing	G7	Es4s	3312–3325.8	14.40	0
5	Lijin	L758	Es3x	3224.3–3250	5.83	–
6	Lijin	LS101	Es4s	4395.1–4448	4.29	46.83
7	Lijin	DF1	Es4s	3104–3250	24.00	–
8	Niuzhuang	W76	Es4s	3262–3340	21.50	0
9	Niuzhuang	Shi13	Es4s	3046.4–3276.5	12.10	0
10	Niuzhuang	He54	Es3x	2928–2964.4	91.30	0.27
11	Niuzhuang	He88	Es3x	3203.6–3214.9	5.89	0
12	Niuzhuang	N52	Es4s	3141.9–3240.5	12.60	–

-: no data.

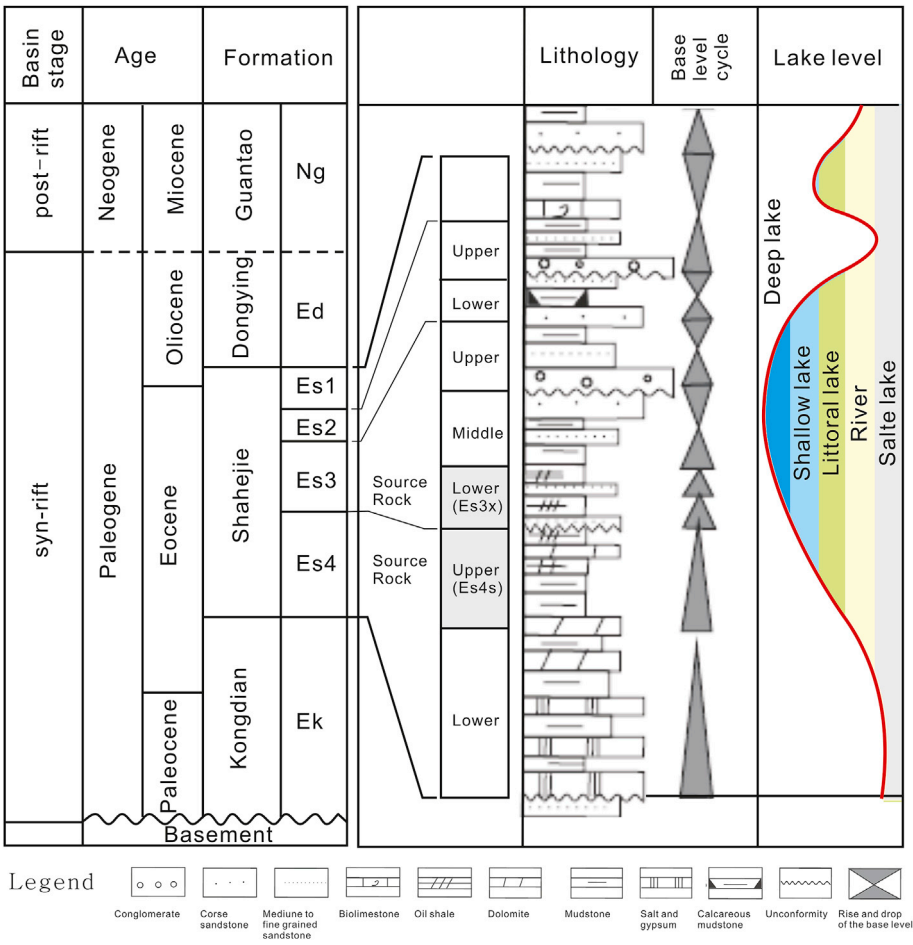

Fig. 2. General stratigraphic column of Shahejie formation (lithology and depositional environments after Feng et al., 2013).

Table 2
General information of the shale oils wellbores.

Well		FY1	LY1	NY1
Stratum	Sub-member	3050–3434 m	3580–3833 m	3300–3500 m
Es3x	1	N=103 3050~3251 m	N=51 3580~3701 m	N=23 3305~3316 m
	2			
	3			
	4			
Es4s	1	N=95 3251–3433.3 m	N=28 3701~3833 m	N=134 3316~3467 m
	2			
	3			
Es4x		~3500 m		>3467 m

Note: N= statistical sample number of stratum interval.

classification scheme presented by Tissot and Welte (1984), GP values greater than 6 mg HC/g indicate good source rock potential. Thus, the classification used to evaluate the quality of source rocks was determined here by plotting GP against TOC (Fig. 4); these results also suggest that high-quality source rocks predominate in the Es3x and Es4s members.

Diagrams that express the relationship between hydrogen index (HI) and maximum temperature (Tmax) are commonly employed to determine and evaluate kerogen types. In this case, the plot shows that our core samples mainly consist of kerogen types I and II (Fig. 5), while a plot of S_2 versus TOC is shown in Fig. 6 and illustrates a rapid decrease in both variables suggesting that both variables in shale decrease as the source rock matures (Jarvie, 2012a). This will also be the case for dead carbon (Conford et al., 1998) and coke due to pyrolysis (Dahl et al., 2004) even though this kerogen type remains oil-prone and in the type I-II kerogen area. Results show that the proportion of dead carbon and coke due to pyrolysis is about 0.8% in our samples, with a little S_2 retained in the matrix.

Rock-Eval results also show that Tmax values are directly correlated with organic matter maturity. Indeed, Tmax values predicted by their relationship with HI mainly fall between 435 °C and 450 °C, within the oil zone (Fig. 5). It is also interesting that the Tmax values of some samples from the Es4s member are obviously less than 435 °C, falling within the immature zone, while those of Es3x samples fall almost within the 'oil window'. Statistical results for vitrinite reflectance (%Ro) versus burial depth (Zhang et al., 2012c) shows that organic matter in the DD enters the 'oil window' at about 2800 m, while the main oil zone is between 3500 m and 4200 m depth. The three shale oil wells discussed here were drilled into the 'early' or 'main oil' zones (Fig. 7) of sulfur-lean source rocks.

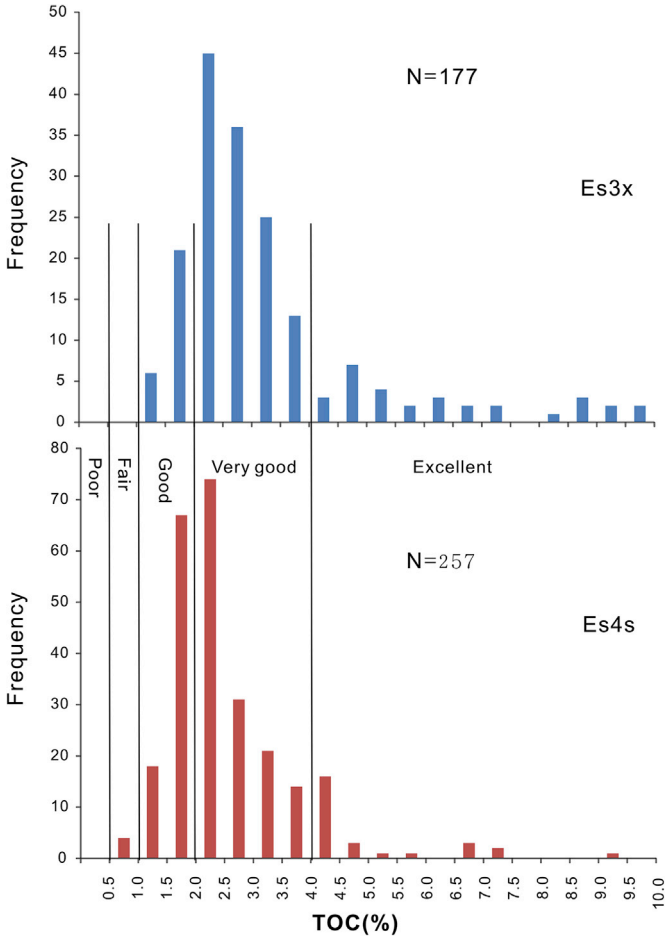

Fig. 3. Frequency distributions of total organic carbon richness of 534 core samples collected from the three shale oil boreholes.

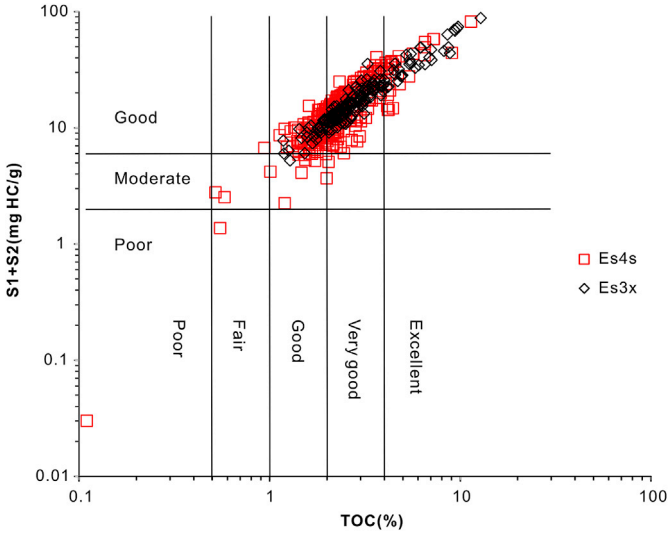

Fig. 4. Total genetic potential (GP) versus the TOC, showing good and very good source rocks predominate.

4.2. Potential for shale oil

On the basis of core samples from three shale oil boreholes, we discuss the potential of three sags within the DD.

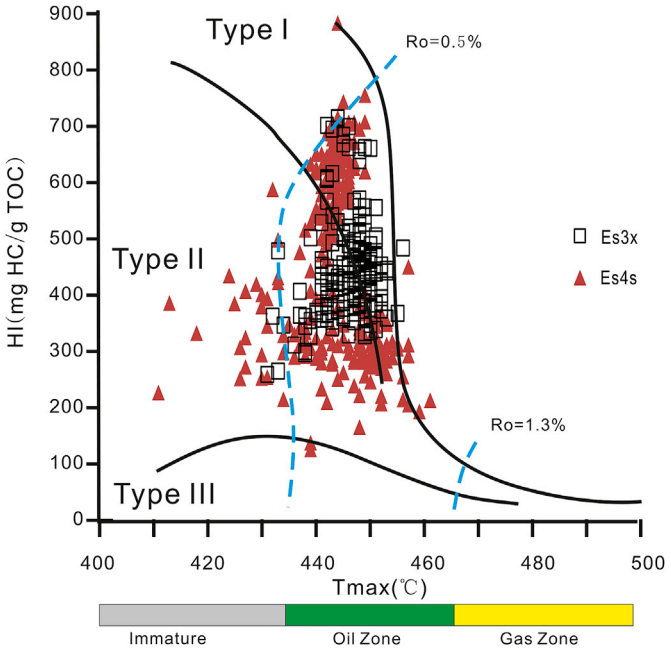

Fig. 5. HI vs. Tmax diagram, showing the samples mainly consisted of kerogen Types I and II and the Tmax values are within "oil window".

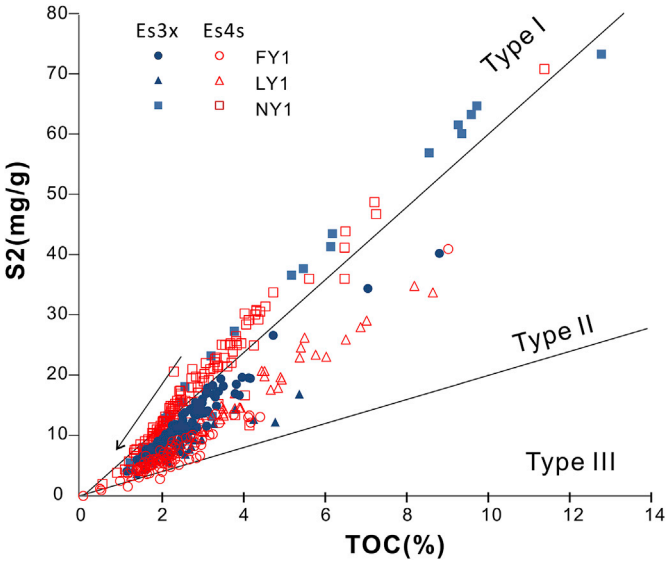

Fig. 6. Rock-Eval S_2 vs, TOC diagram.

In our earlier research (Wei et al., 2012) we have shown that the hydrocarbon (HC) sorption of kerogen is between 120 mg/g TOC and 40 mg/g TOC within the 'oil window' and decreases with maturity. The median value of kerogen HC sorption is thus 80 mg/g TOC, while the sorption of oil onto inorganic minerals is 18.0 mg/g in the case of clay minerals, 3.0 mg/g in the case of quartz and feldspar, and 1.8 mg/g in the case of carbonates. Initial porosity can be estimated to be 50% while current values depend on burial depth; the porosity of the Es3x and Es4s member source rocks clearly decrease as depth increases (Fig. 8) while porosity oscillations occur at depths greater than 3,000 m, very likely caused by hydrocarbon generation (Zhang et al., 2012a). Thus, to simplify this relationship, we used a medium 10% value for porosity to calculate sorption (Sp) at burial depths less than 3500 m and a value of

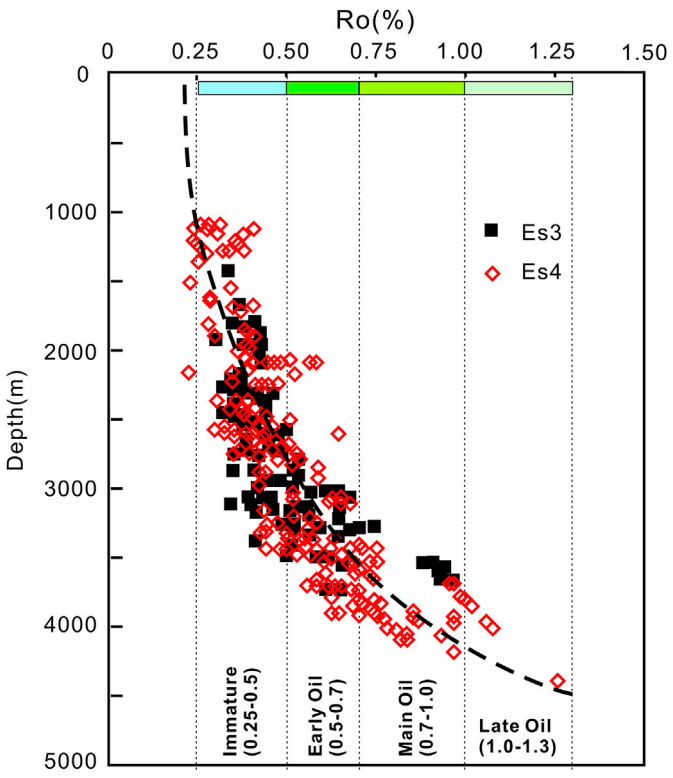

Fig. 7. Statistic vitrinite reflectance (Ro, %) variation with burial depth, the organic matter entering into "oil window" at about 2800 m.

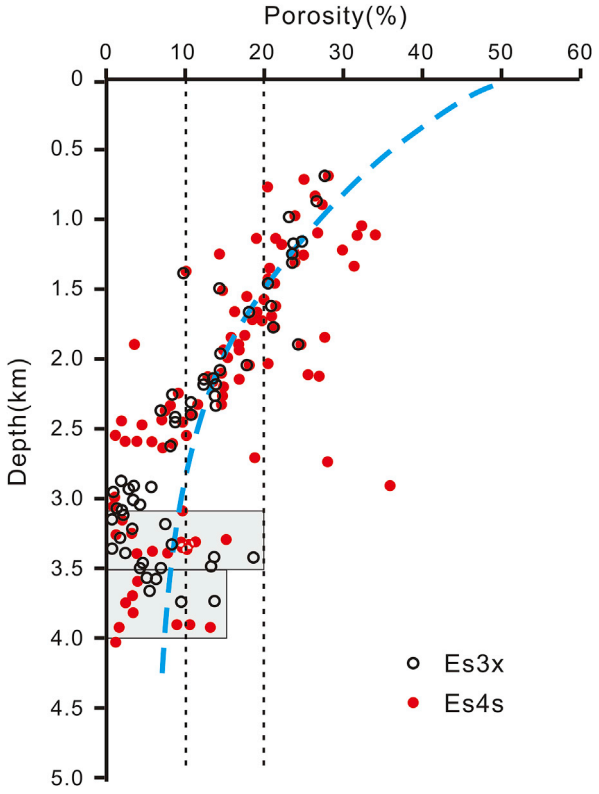

Fig. 8. Variance in present porosity of Es3x and Es4s shale with burial depth, displaying a clear decreasing trend with depth increasing and the porosity oscillations between 3000 and 4000 m.

8% for depths ranging between 3500 and 3800 m. The difference between Sp and Rock-Eval free HC (S_1) was then used as evidence to evaluate the presence, or absence, of free HC; when S_1-Sp is greater than zero, source rocks are oversaturated with free HC, presenting a potential horizon for the production of shale oil.

4.3. The Boxing sag

The Boxing sag is located in the southwest of the DD (Fig. 1) and encompasses shale oil flows recovered from four wells within the Es3x and Es4s members (Table 1). Of these, well FY1 is of particular relevance for shale oil exploration as it was drilled through the main source rocks (i.e., the Es3x and Es4s members) into the Es4x horizon (Table 2), revealing a relatively complete stratigraphic sequence.

In the FY1 profile, average TOC values are 2.6% and 2.2%, respectively, for Es3x and Es4s mudstones and shales. Data from Rock-Eval pyrolysis show that these source rocks are both within the 'oil window' with a Tmax that increases and a HI that decreases as depth increases. The production index (PI, %) of these rocks ranges between 10% and 40% (Fig. 9), with extremely low Tmax values and correspondingly high PI values present in the profile bottom of the third sub-member of Shahejie Formation Es4s strata. A similar set of relationships were observed in the Lou69 well in the neighboring Zhanhua depression (Wang et al., 2015); on the basis of these trends with burial depth, both these wells appear to be affected by HC from early maturated source rocks.

Variations in mineral composition, TOC, Rock-Eval S_1, the oil saturation index (OSI; Jarvie, 2012b), and the oversaturation zone (OSZ) (i.e., S_1-Sp; Li et al., 2016) are illustrated in Fig. 10. Results show that mudstones and shales tend to be rich in carbonate and quartz, more than 30% of their total volume, while the proportions of clay minerals are less than 30%. The relationship between mineral content and depth demonstrates that both quartz and carbonate content increase with depth, while volumes of clay minerals decrease. A weakly positive relationship between quartz content and TOC is also seen, with the exception of the base of this profile, indicating terrigenous silica and nutrient supply. In addition, results demonstrate the presence of a strongly positive correlation between Rock-Eval S_1 and OSI which can easily be understood because the latter is equal to S_1 x 100/TOC (Jarvie, 2012b). Thus, as an approximation, when S_1 is greater than 2.0, the so-called 'oil crossover effect' is seen in almost the whole of this profile, with the exception of the interval between 3170 m and 3210 m. Compared with oil crossover effects, OSZs (Li et al., 2016) occur within two narrow intervals, at the top and bottom of the profile (Fig. 10). Finally, it is interesting that both the OSI and OSZs imply that the region between 3170 m and 3210 m does not represent a potential horizon for shale oil production. When a test run was performed in the region between 3199 m and 3210 m, low flow (2.61 ton/day) combined with cumulative oil production of 9.46 ton were recorded.

4.4. The Niuzhuang sag

One shale oil borehole, the NY1 well, was drilled into the steep slope zone of the Niuzhuang sag within the DD (Fig. 1), encompassing the base of the Es3x member as well as the Es4s and Es4x sub-members of the Shahejie Formation. This borehole revealed the whole of the Es4s horizon at a depth range between 3300 m and 3500 m, and more than 180 core samples were collected separated by approximately 1 m.

Pyrolysis parameters Tmax, HI, and PI versus depth are presented in Fig. 11, and demonstrate that the phenomenon Tmax decreases and PI increases with depth can also be seen in the lower section of this profile. Results show that a depth of 3436 m is the boundary in this profile between the second and third sub-members of the upper part of the fourth member of the Shahejie Formation (Es4s). The third sub-member comprises dark gray mudstones and oil shales intercalated with thin calcitic mudstones and limestones that were deposited in a semi-enclosed saline lacustrine setting. Given this setting, the kerogen source material must

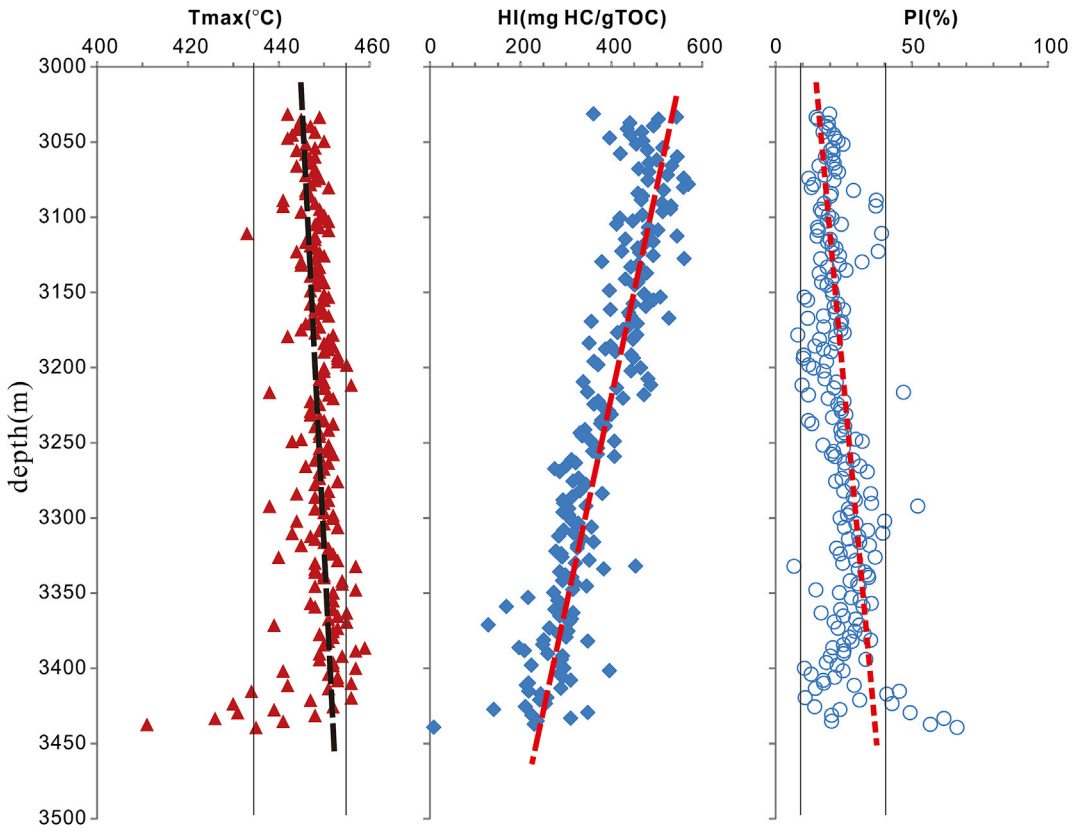

Fig. 9. Rock-Eval parameters vs. depth, showing the shale Tmax and production index (PI, %) increasing, and HI decreasing with depth increasing.

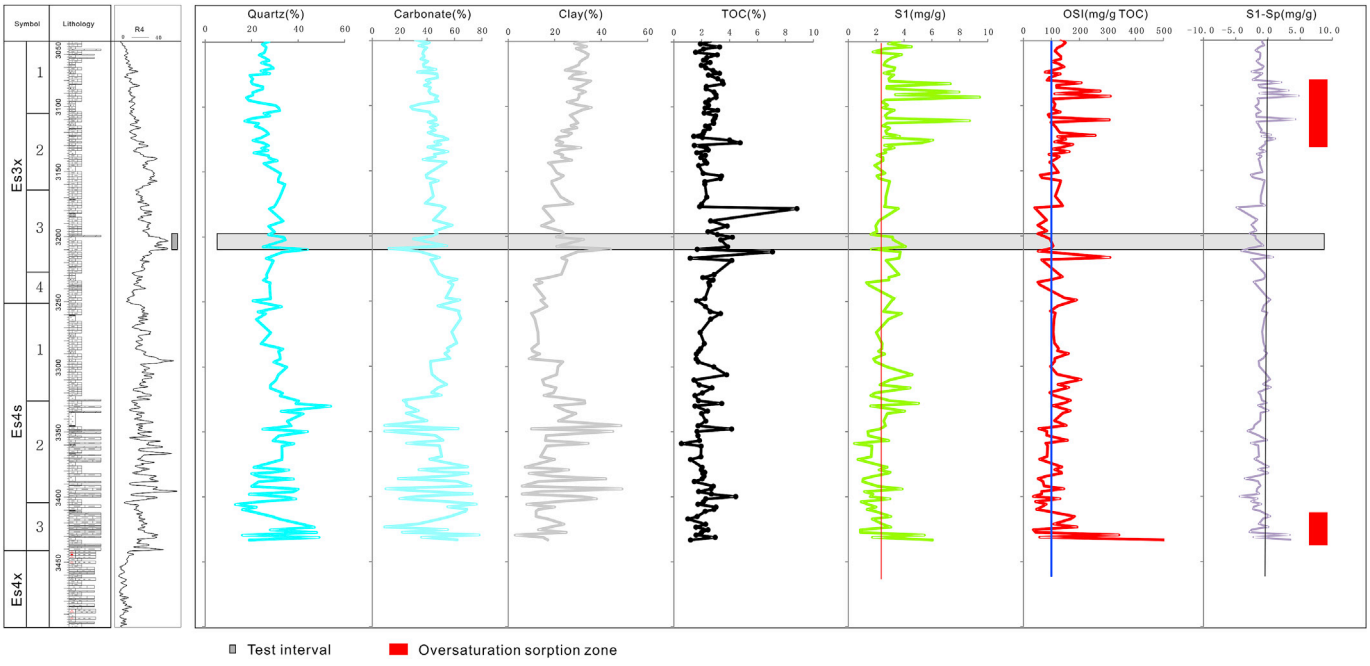

Fig. 10. Variation in the compositions of minerals, TOC, S_1, OSI and oversaturation zone distribution of FY1 profile in Boxing Sag (data after Xie et al., 2016).

have been mixed, originating from aquatic organisms and terrigenous plants. Aquatic organisms were transformed into sulfur-rich kerogen while terrigenous plant debris was altered into type III kerogen over geological time. Previous work has shown that type IS/IIS kerogen reacts at ca. 15 °C lower Tmax temperatures (Conford et al., 1998); thus, at this relatively lower maturity level, sulfur-rich kerogen would have generated hydrocarbons. An earlier biomarker study conducted in a neighboring depression also showed that sulfur rich petroleum is derived from lacustrine carbonate source rocks in the early oil window (Wang et al., 2010). It is well-known that the maturation of organic matter is irreversible, we believe that this process is affected by the early generation of soluble organic matter from sulfur-rich kerogen, leading to the low HI,

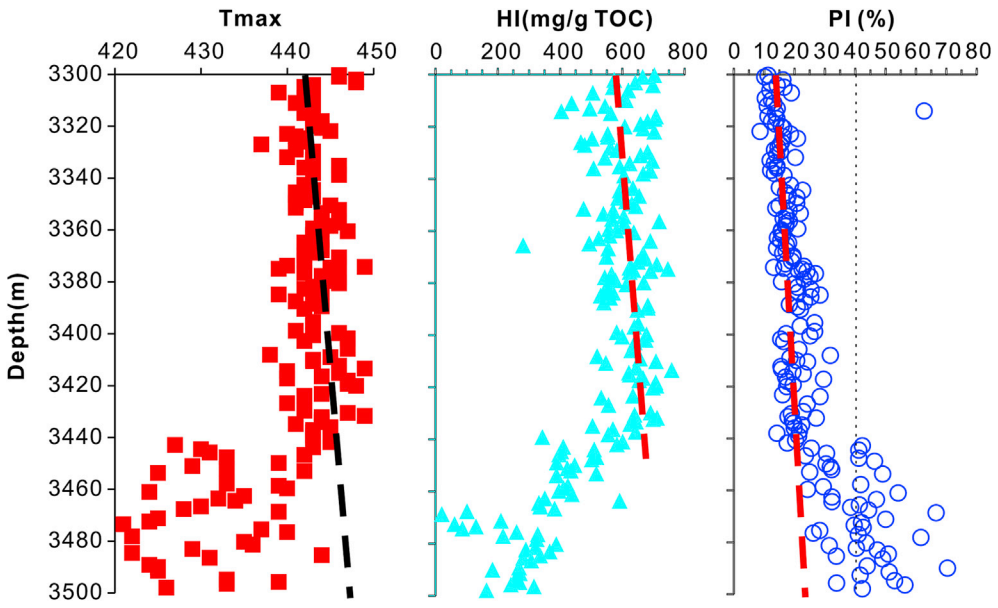

Fig. 11. Tmax, HI and PI versus depth, showing Tmax, HI and PI (%) increasing with depth, and abrupt variation at the lower part of profile.

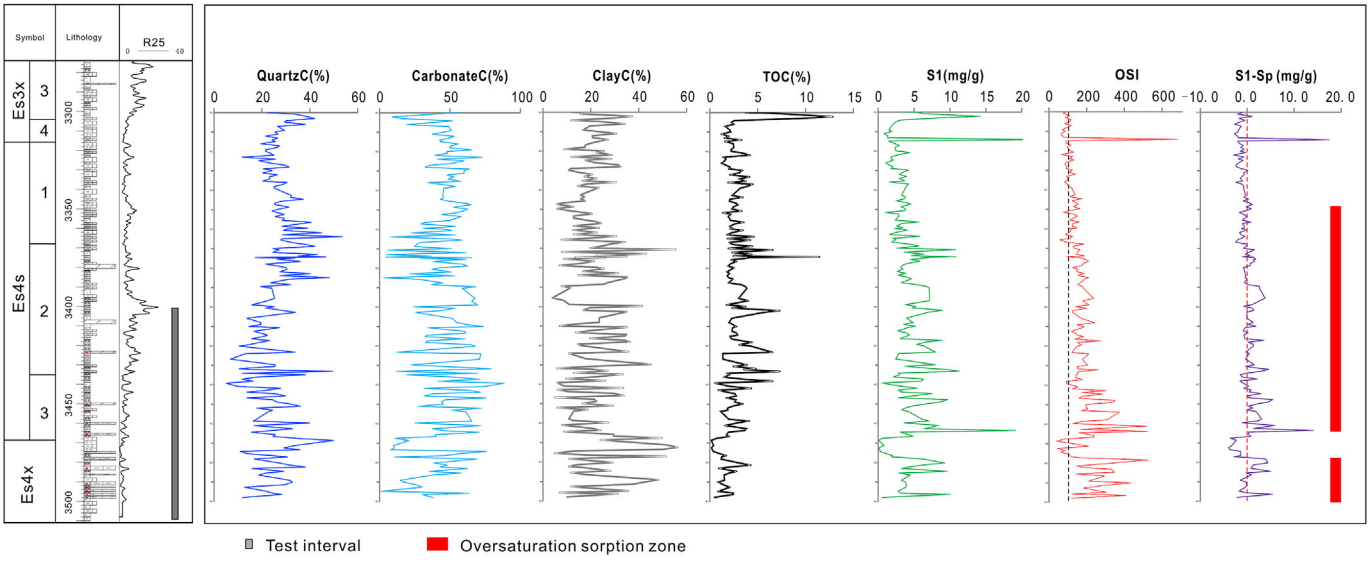

Fig. 12. Variation in the compositions of minerals, TOC, S_1, OSI and oversaturation zone distribution of NY1 profile in Niuzhuang Sag (data after Li et al., 2016; Qi, 2014).

low Tmax, and high PI scenario seen in the basal profile. The hydrocarbons generated early, especially polar components underwent thermal stress. When re-heated in Rock-Eval instrument, they were transformed into HC and released as S_2 of Rock-Eval pyrolysis, which cause Tmax lower shift.

In comparison with the FY1 well, results show a marked difference in HI variation as depth increases. In the former, HI decreases with depth as a result of hydrocarbon generation (Fig. 9), while in the upper section of the NY1 profile a slight increase can be seen with depth or maturity (Fig. 11). Because this effect is uncommon and has not yet been seen in other profiles, it is very likely related to a slight change in upward kerogen composition caused by an increase in the local terrigenous contribution. In other words, aquatic organisms in the lower part of the Es4s strata lead to an increase in hydrocarbon potential (HI), enough to counteract the decrease caused by increasing maturity level. This hypothesis is also supported by basin level cycles (Fig. 2).

Mineral weight percentage compositions of the NY1 profile are characteristic of a high carbonate (average 45.92%), medium quartz (average 25.82%), and low clay (average 21.13%) content. Mineral content versus depth is plotted in Fig. 12 and shows that while relatively high volumes of carbonate and clay minerals characterize the lower parts of the section, below 3370 m, these values clearly fluctuate. Results for S_1, the OSI (Jarvie, 2012b), and the calculated OSZ (Li et al., 2016) indicate that free hydrocarbons exist throughout most of the NY1 profile. In this case, OSZs are mostly below 3340 m, while computed OSZ range is slightly narrower than that of the OSI (Fig. 12). Although both these results imply that this section represents a potential horizon for shale oil production, the test run was carried out at depths between 3,403 m and 3510 m where a stratum thickness of 106 m led to the production of no oil flow. This result may be due of damage to the reservoir and flow blockage caused by use of a heavily water-based drilling fluid; The drilling and completion report for the NY1 well shows that drilling fluid densities used were between 1.34 g/cm^3 and 1.55 g/cm^3 for Es3x and Es4s strata, respectively, while the completion fluid density was 1.65 g/cm^3.

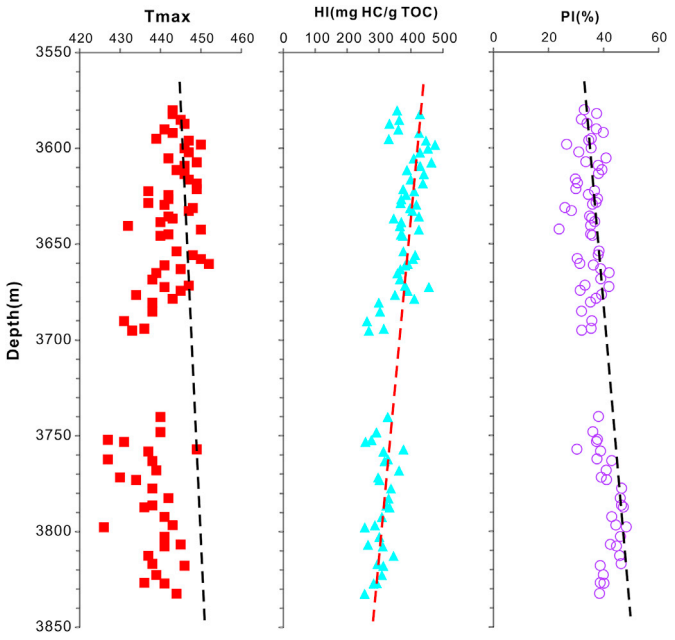

Fig. 13. Tmax, HI and PI versus depth in LY1 profile of Lijin Sag.

4.5. The Lijin sag

The LY1 well is a special borehole that was drilled for shale oil in the Lijing sag. In total, 79 core samples were collected from depths between 3580 m and 3832 m at an average spacing of 2.5 m, while a 50 m spacing interval was used at depths between 3700 m and 3750 m. While a low oil flow (0.29 ton/day) and cumulative production of 0.41 metric tons were obtained from the interval between 3872.6 m and 3899.9 m over the test period, samples could not be collected because the borehole collapsed at the base of the Es4s sub-member after the test run.

Rock-Eval pyrolysis on these core samples was performed, and Tmax, HI, and PI versus depth parameters are presented in Fig. 13 and Table 3. These data exhibit obvious trends such that HI decreases and PI increases at depth, clearly different from the NY1 profile (Fig. 11) and indicating that kerogen was not locally disturbed in this profile. Recorded Tmax values are low between 3650 m and 3840 m in this profile, very similar to the basal regions of the FY1 and NY1 sections (Figs. 9 and 11), and suggesting that this interval is affected by soluble organic matter generated early from sulfur-rich kerogens, which is also supported by the PI versus Tmax diagram (Fig. 14).

The mineral composition of this section and changes with depth are shown in Fig. 15. Results show that while the weight percent carbonate content of this profile is high (average 36.34%), clay content is moderate (average 29.08%), and quartz content is low (average 28.13%). Indeed, in the basal part of this profile, carbonate content is more than 50% while the clay mineral component is less than 30%. Samples with high TOC come from the upper part of this profile, and most are greater than 3%, while values for S_1 are relatively high in the upper section. Oil crossovers (Jarvie, 2012b) are also seen throughout the whole profile, while OSZs (Li et al., 2016) occur within the upper and the lower parts of the profile, with little differences depending on the two methods of prediction (Fig. 15). Comparisons between OSI (Jarvie, 2012b) and sorption potential (Sp; Li et al., 2016) are shown in Fig. 16, and illustrate a major difference when TOC content is low (Fig. 16a). Depending on mineral composition and porosity, Sp is about 2 mg HC/g rock, but because OSI attributes free hydrocarbons to TOC sorption, the former is equal to zero when TOC is also zero. The difference between these two variables decreases when free HC (i.e., S_1) or TOC is relatively high (Fig. 16b). Nevertheless, 'cross point' occurred at a TOC value of about 10% (Fig. 16), caused by OM sorption in OSI and Sp. While the OSI is simple

Table 3
TOC and Rock-Eval data of Well LY1.

Depth (m)	Stratum	TOC (wt., %)	S1 (HC mg/g)	S2 (HC mg/g)	Tmax (°C)	HI (HC mg/g TOC)
3580.17	Es3x	3.04	5.35	10.86	443	357.24
3582.14	Es3x	2.73	7.02	11.70	443	428.57
3585.14	Es3x	3.17	5.42	11.52	445	363.41
3587.18	Es3x	1.19	2.04	3.96	446	332.77
3590.13	Es3x	2.72	5.85	9.81	441	360.66
3592.03	Es3x	2.99	8.47	12.74	443	426.09
3595.11	Es3x	2.11	3.85	6.98	439	330.81
3596.04	Es3x	3.82	9.05	17.08	447	447.12
3598.15	Es3x	5.53	9.55	26.31	450	475.77
3600.10	Es3x	5.44	13.59	24.68	446	453.68
3602.17	Es3x	2.70	5.21	11.57	447	428.52
3605.27	Es3x	3.27	9.26	13.38	442	409.17
3607.30	Es3x	4.48	10.53	20.81	449	464.51
3609.16	Es3x	3.49	9.21	14.97	446	428.94
3611.36	Es3x	3.54	8.95	13.73	444	387.85
3613.38	Es3x	3.06	8.33	13.49	446	440.85
3616.23	Es3x	4.94	8.38	19.74	447	399.60
3618.29	Es3x	4.55	8.76	19.91	449	437.58
3621.26	Es3x	4.70	7.57	17.67	449	375.96
3622.33	Es3x	2.59	6.18	10.62	437	410.04
3624.31	Es3x	2.89	5.87	11.13	442	385.12
3626.47	Es3x	3.96	8.92	14.66	442	370.20
3628.48	Es3x	2.53	5.54	9.31	437	367.98
3629.43	Es3x	2.98	7.01	12.44	441	417.45
3631.09	Es3x	6.54	9.14	26.02	448	397.86
3632.71	Es3x	5.80	9.29	23.47	447	404.66
3635.56	Es3x	5.41	12.36	23.00	442	425.14
3636.58	Es3x	3.08	5.93	10.67	443	346.43
3638.48	Es3x	2.94	6.34	10.88	440	370.07
3640.50	Es3x	2.65	5.30	9.69	432	365.66
3642.37	Es3x	8.22	10.97	34.95	450	425.18
3644.95	Es3x	4.88	9.82	17.99	442	368.65
3645.67	Es3x	3.93	8.26	14.73	440	374.81
3653.78	Es3x	3.55	8.33	13.36	444	376.34
3655.72	Es3x	7.05	17.94	29.16	448	413.62
3657.75	Es3x	6.90	12.33	28.09	450	407.10
3660.28	Es3x	8.67	15.50	33.85	452	390.43
3661.08	Es3x	3.82	8.34	14.60	441	382.20
3663.08	Es3x	3.47	8.13	12.74	445	367.15
3665.14	Es3x	3.02	7.86	10.82	439	358.28
3668.38	Es3x	2.69	6.29	9.83	438	365.43
3671.64	Es3x	6.06	11.55	23.13	447	381.68
3672.38	Es3x	4.55	15.03	20.78	441	456.70
3674.34	Es3x	4.97	8.93	19.38	445	389.94
3676.52	Es3x	2.47	5.61	8.65	434	350.20
3678.54	Es3x	3.54	8.65	14.55	443	411.02
3680.52	Es3x	2.37	3.87	7.10	438	299.58
3685.20	Es3x	2.27	3.25	6.89	438	303.52
3690.20	Es3x	1.28	1.87	3.36	431	262.50
3694.16	Es3x	1.87	3.24	5.89	436	314.97
3695.17	Es3x	1.53	1.94	4.11	433	268.63
3740.17	Es4s	2.23	4.51	7.30	440	327.35
3748.10	Es4s	1.64	2.71	4.79	440	292.07
3752.13	Es4s	1.60	2.69	4.42	427	276.25
3753.16	Es4s	1.42	2.19	3.66	431	257.75
3757.16	Es4s	3.83	6.29	14.44	449	377.02
3758.19	Es4s	1.91	3.83	6.00	437	314.14
3762.29	Es4s	1.32	2.61	4.33	427	328.03
3763.21	Es4s	2.44	5.84	7.75	438	317.62
3768.15	Es4s	3.31	8.35	12.02	439	363.14
3771.81	Es4s	4.28	8.21	12.74	430	297.66
3773.10	Es4s	1.82	3.83	5.49	434	301.65
3777.53	Es4s	2.02	5.95	6.82	438	337.62
3782.63	Es4s	2.83	8.00	9.35	442	330.39
3786.35	Es4s	2.24	6.30	7.24	438	323.21
3787.36	Es4s	2.05	6.12	6.84	436	333.66
3792.36	Es4s	2.44	5.68	7.54	441	309.02
3796.72	Es4s	2.71	6.24	7.79	443	287.45
3797.74	Es4s	4.81	11.47	12.29	426	255.51
3802.75	Es4s	2.75	7.10	8.28	441	301.09
3806.81	Es4s	2.61	5.13	6.94	445	265.90
3807.75	Es4s	3.01	7.60	9.39	441	311.96
3812.73	Es4s	2.51	7.35	8.68	437	345.82

(*continued on next page*)

Table 3 (*continued*)

Depth (m)	Stratum	TOC (wt., %)	S1 (HC mg/g)	S2 (HC mg/g)	Tmax (°C)	HI (HC mg/g TOC)
3816.89	Es4s	2.15	5.50	6.35	438	295.35
3817.87	Es4s	5.40	10.75	16.94	446	313.70
3822.75	Es4s	1.62	3.33	5.01	439	309.26
3826.83	Es4s	2.52	4.69	7.39	436	293.25
3827.05	Es4s	2.15	4.09	6.09	441	283.26
3832.44	Es4s	2.21	3.53	5.63	444	254.75

Note: production index (PI) can be calculated from Rock-Eval data, i.e., PI=S1/(S1+S2), when necessary.

and easy to use, the OSZ is comprehensive and is associated with mineral composition as well as the components and properties of organic matter. Thus, the former is suited for relatively high TOC (>1.0) and an early-medium maturity level due to the high levels of sorption used, while the latter is based on whole rocks and is more appropriate for wider TOCs and maturity levels when localized, variable sorptions are applied.

4.6. The potential distribution of shale oil

The known distribution of flowing oil wells (Table 1, Wang et al., 2013) and the special boreholes drilled for shale oil discussed in this paper are shown in Fig. 17. These boreholes illustrate the relationship between drilled depth and maturity level in shale rocks and show that they are predominantly within the early 'oil window', shallower than 3500 m in depth. In addition, a few wells were also drilled into strata deeper than 3500 m, referred to as the main 'oil window' or late 'window' (Fig. 17). Generally, because crude oils generated within the early 'oil window' contain a relatively high asphaltene content and have high viscosity and weak mobility, their migration paths in shales are often blocked by asphaltene. As a result, steady oil flows can rarely be obtained. Because of this effect, it has been suggested that target strata for shale oil exploration within the DD should be greater than 3400 m in depth (Li et al., 2016).

Taking into account the burial depth and maturity level of rocks within the Es3 and Es4 members, the potential distribution of shale oil can be predicted. The potential distribution of Es3 shale oil (Fig. 18) shows that relatively large areas of these rocks can be classified within the main 'oil window' in the Lijin and Boxing sags, while a much smaller area is encapsulated by the Niuzhuang Sag. The potential distribution of shale oil within the Es4 member is shown in Fig. 19, suggesting areas of this main 'oil window' are a little extended within the Niuzhuang and Boxing sags. Nevertheless, because the main 'oil window' area comprised by the Es4 shale is not large enough compared with the Lijin Sag, our results suggest that there is less risk to shale oil exploration within deep

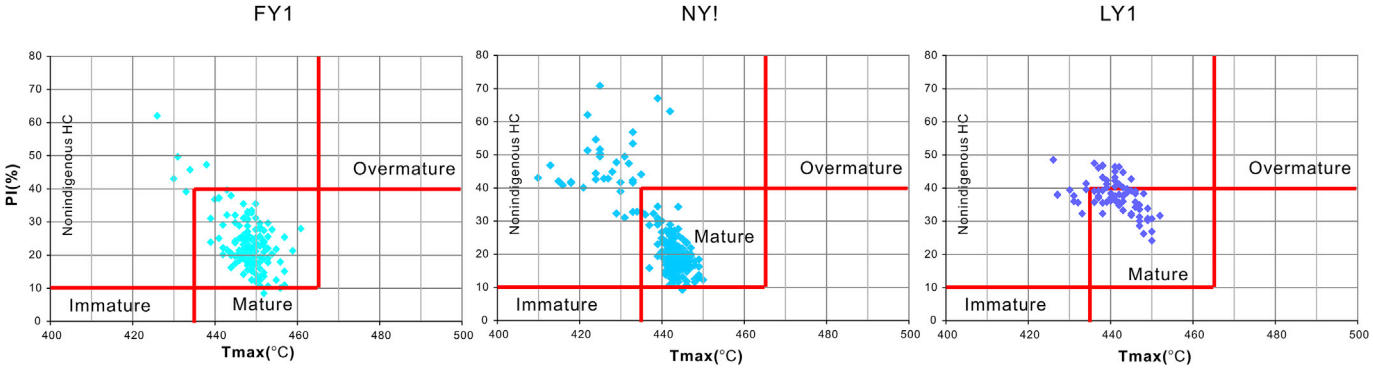

Fig. 14. PI vs Tmax diagrams showing nonindigenous HC effect.

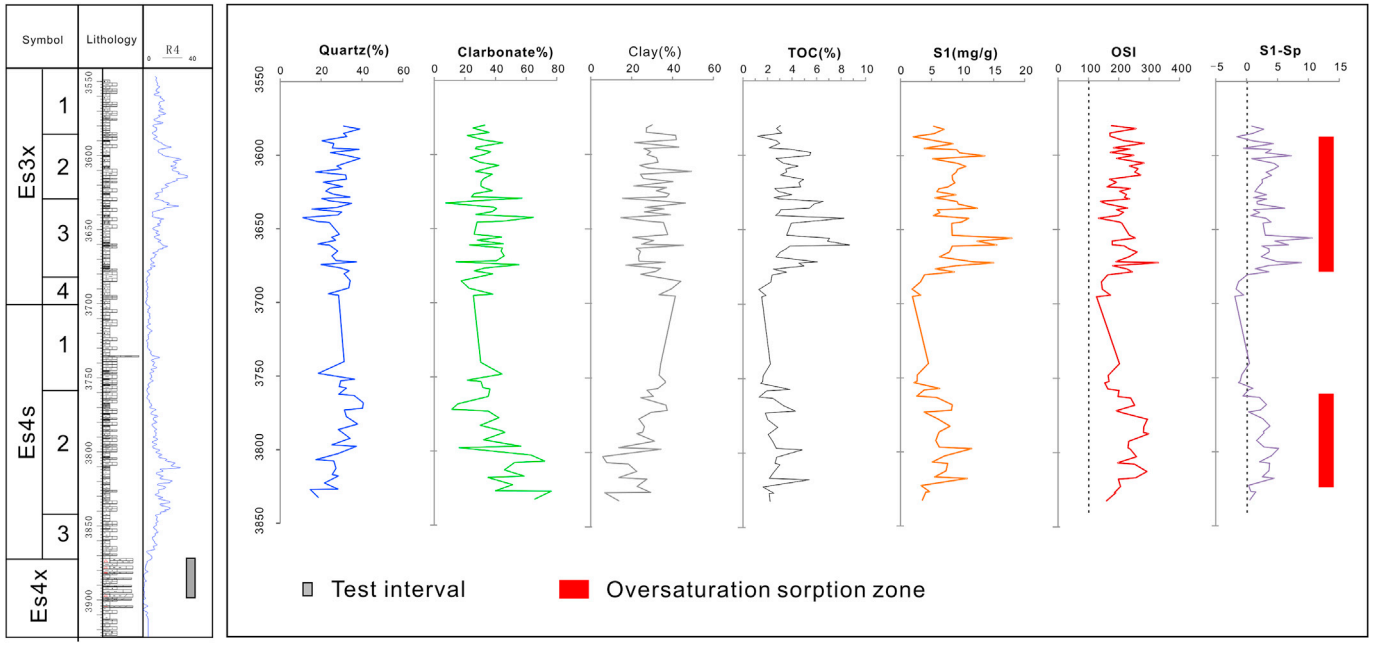

Fig. 15. Mineral compositions, TOC, S_1, OSI and oversaturation zone distribution changes with depth in LY1 profile of Lijin sag.

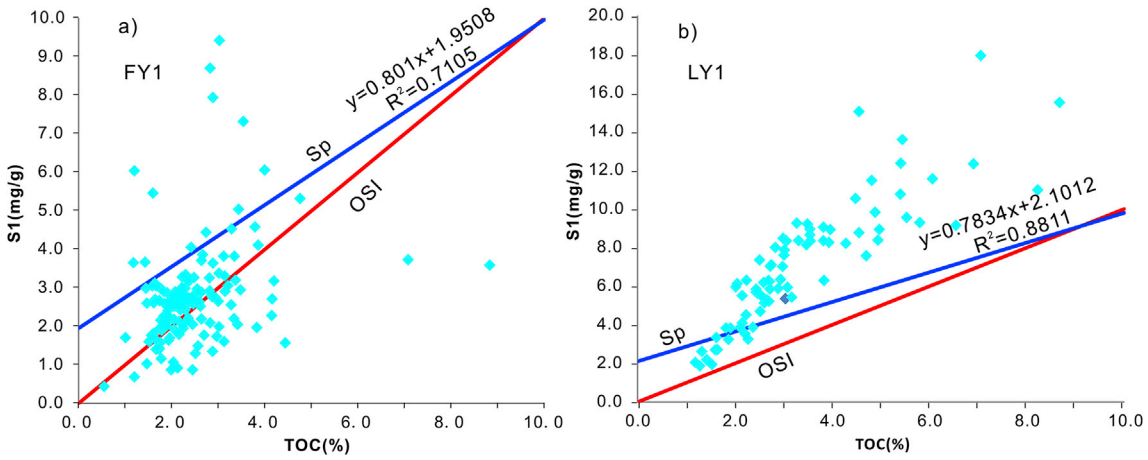

Fig. 16. Contrast diagrams of OSI and Sp on S_1 versus TOC of FY1 profile (a) and LY1 profile (b), Sp showing an about 2 mg/g Rock sorption potential.

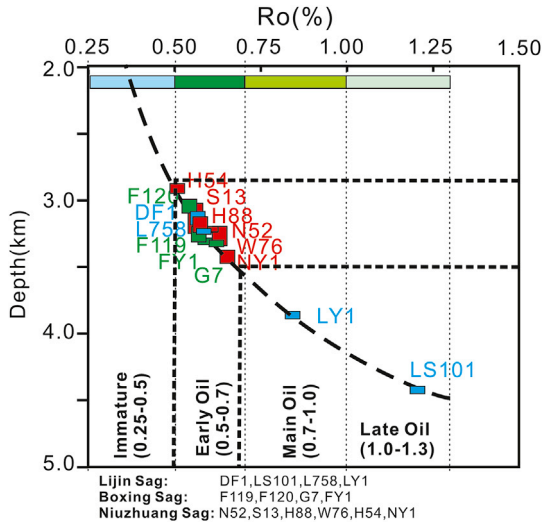

Fig. 17. Variance of the know shale oil/gas wells with the buried depth and maturity.

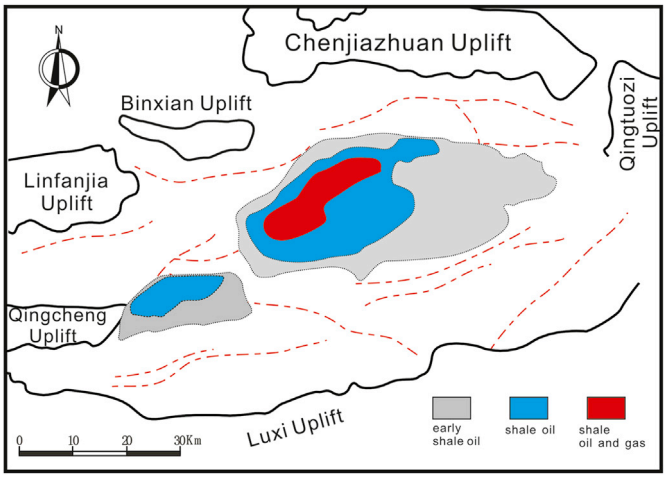

Fig. 18. Potential distribution of shale oil in the Es3x strata of the Dongying Depression.

shale strata of the Es3 and Es4 members at burial depths greater than 3400 m as well as the maturity level of the main 'oil window' attained in the Lijin and Boxing sags. Thus, further exploration of the Niuzhuang Sag

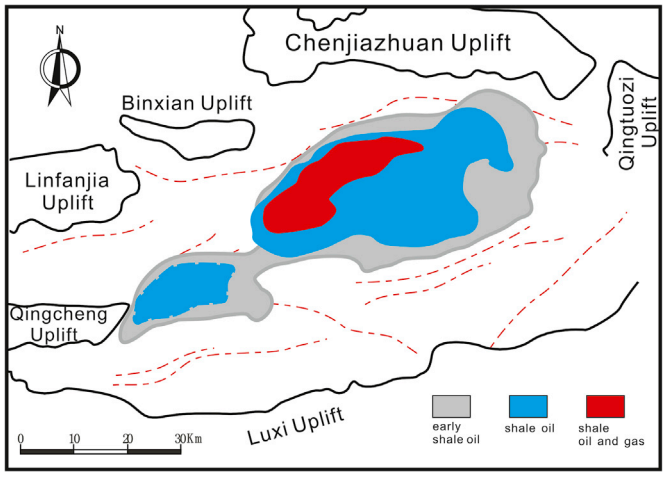

Fig. 19. Potential distribution of shale oil in the Es4s strata of the Dongying Depression.

would not be a viable option to preserve the shale oil of the DD.

5. Conclusions

Shale oil exploration within the DD of the BBB was initiated in 2013, and to date three boreholes (i.e., FY1, NY1, and LY1) targeted at the exploration of shale oil have been drilled in the Boxing, Niuzhuang, and Lijing sags. In each case, the goal horizons were set as the Es3x and Es4s mudstones and shales within these sags, and all three boreholes demonstrate a high shale oil potential for both horizons on the basis of the distribution of OSZs. These differences between OSI and OSZ occur because mineral oil sorption is taken into account in Sp calculations; indeed, when TOC and S_1 are low, this difference is obvious, while very low Tmax values in profiles are affected by soluble organic matter generated early from sulfur-rich kerogen while the HI increase with depth and maturation in the NY1 profile is caused by an increase in light aquatic organic matter.

Shale oil flows discovered in some wells drilled for conventional exploration corroborate the high shale oil potential of the Es3x and Es4s horizons within the DD, even though most boreholes did not reach the main 'oil window' in shale strata. The results of this study therefore imply that the goal horizons for shale oil exploration within the DD should be determined when the depth of the Es3 and Es4 members are greater than 3400 m, where exploration risk is less. The Lijin and Boxing sags should also be prioritized for shale oil expiration within the DD, while regions with relatively gentle slopes should be considered for future investigation

as these comprise larger areas of mature mudstones and shales and therefore will provide more oil supply than steeper slopes.

Acknowledgments

We gratefully acknowledge the National Basic Research Program of China (Grant No. 2014CB239100) and the NSFC of China (Grant No. 41173054; 41072096; 41372129) for financial support. Thanks are given to two anonymous reviewers for their comments and constructive suggests.

References

Allen, M.B., McDonald, D.I.M., Zhao, X., Vincent, S.J., Brouet-Menzies, C., 1997. Early Cenozoic two-phase extension and late Cenozoic thermal subsidence and inversion of the Bohai basin, northern China. Mar. Petroleum Geol. 14, 951–972.

Conford, C., Gardner, P., Burgess, C., 1998. Geochemical truths in large data sets. I: geochemical screening data. Org. Geochem. 29, 519–530.

Dahl, B., Bojesen-Koefoed, J., Holm, A., Justwan, H., Rasmussen, E., Thomsen, E., 2004. A new approach to interpreting Rock-Eval S2 and TOC data for kerogen quality assessment. Org. Geochem. 35 (11–12), 1461–1477.

Espitalie, J., Deroo, G., Marquis, F., 1985. La pyrolyse rock-eval et ses applications. Partie 1. Rev. 1'lnstitut Francois Pet. 40 (5), 563–579.

Feng, Y., Li, S., Lu, Y., 2013. Sequence stratigraphy and architectural variability in late Eocene lacustrine strata of the dongying depression, Bohai Bay Basin, eastern China. Sediment. Geol. 295, 1–26.

Jarvie, D.M., 2012a. Shale resource systems for oil and gas: Part 1—shale-gas resource systems. In: Breyer, J.A. (Ed.), Shale Reservoirs—Giant Resources for the 21st Century: AAPG Memoir 97, pp. 69–87.

Jarvie, D.M., 2012b. Shale resource systems for oil and gas: part 2—shale–oil resource systems. In: Breyer, J.A. (Ed.), Shale Reservoirs—giant Resources for the 21st Century. AAPG Memoir 97, pp. 89–119.

Li, Z., Zou, Y.-R., Xu, X., Sun, J.-N., Li, M., Peng, P., 2016. Adsorption of mudstone source rock for shale oil — experiments, model and a case study. Org. Geochem. 92, 55–62.

Peters, K., Cassa, M.R., 1994. Applied source rock geochemistry. In: Magoon, L.B., Dow, W.G. (Eds.), The Petroleum System—from Source to Trap. AAPG Memoir 60, pp. 93–120.

Qi, Y., 2014. Study on organic geochemical characteristics of Niuye-1 well in dongying SAG. Neijiang Sci. Technol. 11, 64–66 (in Chinese).

Tissot, B.P., Welte, D.H., 1984. Petroleum Formation and Occurrence, second ed. Berlin Heidelberg New York, Tokyo, Springer-Verlag, p. 699.

Wang, M., Wilkins, R.W.T., Song, G., Zhang, L., Xu, X., Li, Z., Chen, G., 2015. Geochemical and geological characteristics of the Es3l lacustrine shale in the Bonan sag, Bohai Bay Basin, China. Int. J. Coal Geol. 138, 16–29.

Wang, Y., Li, Z., Gong, J., Zhu, J., Hao, Y., Hao, X., Wang, Y., 2013. Discussion on an evaluation method of shale oil and gas in Jiyang Depression: a case study on Luojia area in Zhanhua Sag. Acta Pet. Sin. 34 (1), 83–92 (in Chinese with English abstract).

Wang, G., Wang, T.G., Simoneit, B.R.T., Zhang, L., Zhang, X., 2010. Sulfur rich petroleum derived from lacustrine carbonate source rocks in Bohai Bay Basin, East China. Org. Geochem 41, 340–354.

Wei, Z., Zou, Y.-R., Cai, Y., Wang, L., Luo, X., Peng, P., 2012. Kinetics of oil group-type generation and expulsion: an integrated application to Dongying Depression, Bohai Bay Basin, China. Org. Geochem. 52, 1–12.

Xie, X., Li, M., Littke, R., Huang, Z., Ma, X., 2016. Petrographic and geochemical characterization of microfacies in a lacustrine shale oil system in the Dongying Sag, Jiyang Depression, Bohai Bay Basin, Eastern China. Int. J. Coal Geol. 165, 49–63.

Zhang, L., Li, J., Li, Z., Zhang, J., Zhu, R., Bao, Y., 2014. Advances in shale oil/gas research in North America and considerations on exploration for continental shale oil/gas in China. Adv. Earth Sci. 29, 700–711 (in Chinese with English abstract).

Zhang, L., Li, Z., Li, J., Zhu, R., Sun, X., 2012a. Feasibility analysis of existing recoverable oil and gas resource in the palaeogene shale of Dongying depression. Nat. Gas. Geosci. 23, 1–13 (in Chinese with English abstract).

Zhang, S., Wang, Y., Zhang, L., Li, Z., Zhu, J., Gong, J., Hao, Y., 2012b. Formation conditions of shale oil and gas in Bonan sub-sag, Jiyang depression. China Engi. Science 14, 49–55 (in Chinese with English abstract).

Zhang, S., Zhang, L., Li, Z., Hao, Y., 2012c. Formation conditions of Paleogene shale oil and gas in Jiyang depression. Petroleum Geol. Recovery Effic. 19 (2), 1–5 (in Chinese with English abstract).